SCIENCE CHINA
Earth Sciences

• RESEARCH PAPER •

doi: 10.1007/s11430-013-4630-5

Magmatism and tectonic processes in Area A hydrothermal vent on the Southwest Indian Ridge

ZHANG Tao[1,2*], LIN Jian[3] & GAO JinYao[1,2]

[1] *Second Institute of Oceanography, State Oceanic Administration, Hangzhou 310012, China;*
[2] *Key Laboratory of Submarine Geosciences, State Oceanic Administration, Hangzhou 310012, China;*
[3] *Department of Geology and Geophysics, Woods Hole Oceanographic Institution, Woods Hole, MA 02543, USA*

Received October 8, 2012; accepted February 20, 2013

The hydrothermal vent in Area A (37.78°S, 49.65°E) is the first active hydrothermal vent discovered on the Southwest Indian Ridge (SWIR). Heat source and adequate bulk permeability are two necessary factors for the formation of a hydrothermal vent. Along the SWIR 49.3°E to 51.2°E, the gravity-derived crustal thickness is up to 9.0 km, much thicker than the average thickness of the global oceanic crust. This characteristic indicates that the magma supply in this area is robust, which is possibly affected by a hotspot. The large-scale residual mantle Bouguer anomalies (RMBA) reveal prominent negative-gravity anomalies between the first-order ridge segment (from Indomed to Gallieni, 46.0°E to 52.0°E) and the Marion-Del Cano-Crozet region. These anomalies indicate the channel of the hotspot-ridge interaction. The tomography data corrected with theoretical thermal model indicate that the low-velocity anomalies corresponding to this channel can reach the base of the lithosphere. Near the hydrothermal vent area, the topography and crustal thickness at the off-axis area are extremely asymmetrical. South of the SWIR, the high topography corresponds to the thinning crustal thickness. The residual isostatic topography anomalies indicate that Area A is a deviation from the local isostatic equilibrium, similar to the characteristics of the transform fault inside corner. The forward profiles of the magnetic data indicate that the thinning magnetic layer at the south side of Area A corresponds to the shallow, high-velocity area revealed by the OBS, which is the result of tectonic extension of a detachment fault. The active tectonic processes in Area A can provide sufficient crustal permeability to the hydrothermal circulation and may form massive sulfide deposits.

ultra-slow spreading ridge, Area A hydrothermal vent, RMBA, hotspot-ridge interaction, detachment fault

Citation: Zhang T, Lin J, Gao J Y. Magmatism and tectonic processes in Area A hydrothermal vent on the Southwest Indian Ridge. Science China: Earth Sciences, 2013, doi: 10.1007/s11430-013-4630-5

The spreading rate of mid-ocean ridge is the primary control factor of magmatism at the seafloor spreading center. Along ultra-slow spreading ridge (full spreading rate is less than 20 mm/a), magmatism is significantly attenuated and may be completely absent in some area (Dick et al., 2003). The decreased magmatic budget limits the incidence of hydrothermal vents on the ultra-slow spreading ridge. The ultra-slow spreading ridge consists mainly of the Southwest Indian Ridge (SWIR) and the Arctic Gakkel ridge, and accounts for 20% of the total length of the global mid-ocean ridge. Nevertheless, it was not until 2007 that China's R/V DaYang Yi Hao observed the first active hydrothermal vent (Area A hydrothermal vent) in the SWIR in DY-19 cruise (Tao et al., 2012). The location of the Area A vent is presented in Figure 1.

Zhu et al. (2010) suggested that the total low crustal magnetization zone is approximately 9×10^4 m^2, even larger than that of the TAG area, by analyzing the near-bottom

*Corresponding author (email: zhangtaosio@gmail.com)

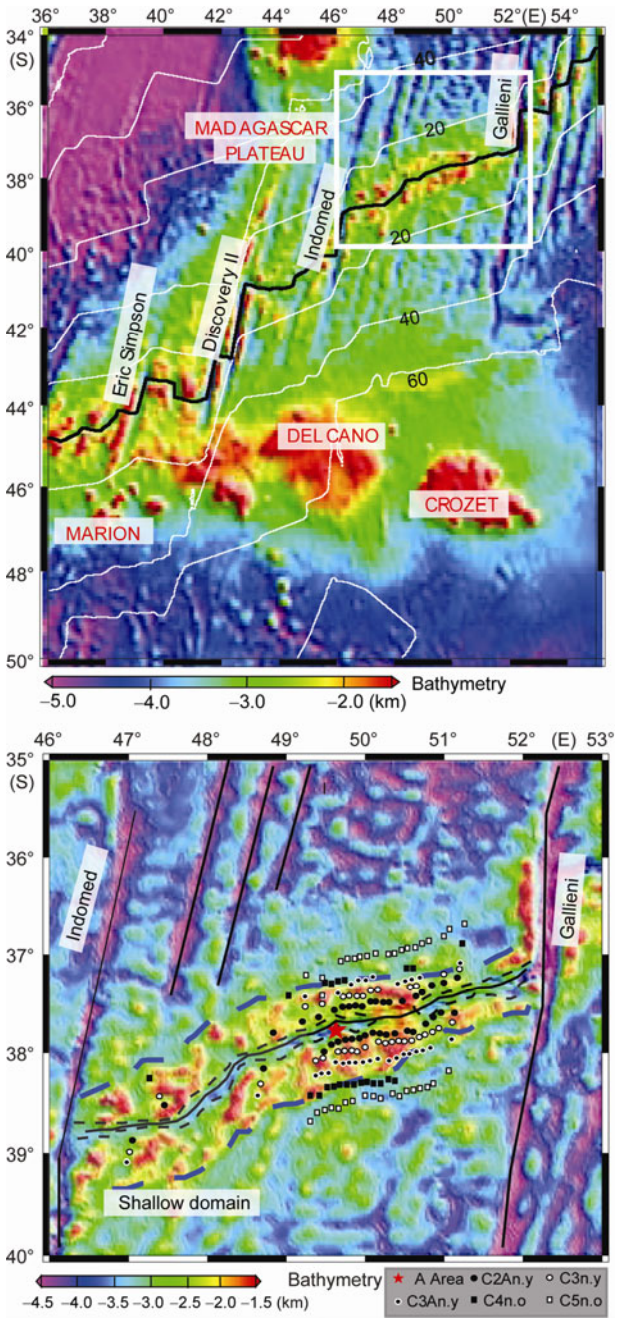

Figure 1 Bathymetry of the study area. (a) Hotspots and plateaus are indicated in red. Large transform faults are in black. The white contours delineate the crustal age with 20 Ma intervals and are labeled in black. The location of the spreading center is shown as a black solid line. The white box outlines the region of (b), whereas the outer edge of the shallow domain and the mid-ocean ridge discontinuities are shown as the blue dotted line and the black solid line, respectively (b). The identifications of the magnetic lineations are modified from Sauter et al. (2009).

magnetic data above the Area A hydrothermal vent. There should be adequate heat sources and sufficient permeability to support such an intensive hydrothermal vent (Baker et al., 2004). Area A is located on the segment between Indomed and Gallieni transform faults (46.0°E to 52.0°E). Compared with its east and west sides, this segment has a shallow depth, which is completely different from the traditional understanding of ultra-slow spreading ridges. The thickened crust and the robust magmatism in this area were documented in the global cruise (DY115-17A) in 2005 (Lin et al., 2006). This phenomenon is also supported by the OBS data collected by Chinese researchers in the SWIR (Zhao et al., 2011; Ruan Aiguo, Personal Communication). The mean axial depth of the 46.0°E to 52.0°E segment is 3 km shallower than the SWIR 9°E to 16°E and 57°E to 70°E regions (Dick et al., 2003; Cannat et al., 2006). The crustal thickness is up to 9.0 km, which significantly deviates from the model of the relationship between spreading rate and crustal thickness. In 2009, by analyzing the bathymetry, gravity and other geophysical data since C5n.o, Sauter et al. (2009) suggested that this area may be related to the Crozet hotspot since 11–8 Ma.

Aimed at the heat source and crust permeability of the Area A vent, the issues in this study are as follows: (1) Are the heat sources of the Area A hydrothermal vent and the shallow domain along the entire 46.0°E to 52.0°E segment related to the Crozet hotspot? (2) If it is, where is the hotspot-ridge interaction channel? (3) What are the tectonic processes of the Area A vent? The first two questions are related to the heat source of the hydrothermal vent, whereas the third one is related to the crust permeability. Large-scale RMBA and residual tomography data corrected with the theoretical thermal model are calculated using bathymetry, gravity, and tomography data to address the above questions. The results are used to reveal the process and channel of the hotspot effect along the SWIR. The crustal thickness, the residual topography, and the thickness of the magnetic source layer are calculated to reveal the isostatic compensation and tectonic features of the Area A vent zone.

1 Regional setting

1.1 The Interaction of SWIR and hotspots

Mid-ocean ridge and hotspots are two surface manifestations of magmatism caused by mantle upwelling. When mid-ocean ridge and hotspots are within a close distance, their interaction usually leads to tremendous physical and chemical anomalies (Ito et al., 2003). Ito et al. (2003) posited that over 15% of global mid-ocean ridges are affected by hotspots. Moreover, recent research showed that over 30% of MAR is associated with hotspots (Wang et al., 2011). The mid-ocean ridges near hotspots generally have shallower water depths, thickened crusts, and corresponding geochemical anomalies. Along the mid-ocean ridge, the propagation of the hotspot effect often constructs a V-shaped region, which gradually narrows from the part near the hotspot down to the far distance.

There are two hotspots near the SWIR, namely, Marion and Crozet. Marion's effect on the SWIR (especially on the 46.0°E to 52.0°E area) has gradually decreased since 42 Ma

(Zhang et al., 2011). At present, Marion is more than 1200 km away from the Area A vent, close to or greater than the maximum theoretical ridge-hotspot interaction distance. Based on the RMBA along the SWIR, Georgen et al. (2010) suggested that the effect of Marion is blocked by the Discovery II transform fault; thus, the effect along the SWIR east of Discovery II is reduced or has disappeared. The Crozet plateau is shallower than the adjacent Del Cano Rise and is regarded as the position of the present mantle plume (Recq et al., 1998). However, compared with Marion, its origin, track, and activities are still a subject of considerable debate. Montelli et al. (2004) suggested that Crozet and Kerguelen both originated from the plume 2350 km deep lying north of Crozet Islands. Owing to the similar distance and track of the Conrad and Kerguelen hotspots, the origin and track of the Crozet hotspot have been a topic of debate. Volcanism occurred on the Crozet Islands for the last 9 Ma and produced OIB-type lavas (Sauter et al., 2009). The seismic velocity in the crust of the Crozet plateau is similar to that of the Kerguelen plateau (Recq et al., 1998; Charvis et al., 1995). The crustal thickness determined by the seismic (10–16.5 km) is consistent with the average crustal thickness of a plume-affected area. The gravity model shows that the Crozet plateau was created on the relatively cold, late Mesozoic lithosphere and may be supported by the active thermal anomaly (Goslin et al., 1984; Curray et al., 1991).

1.2 The topographic anomaly on 46.0°E to 52.0°E Segment

The topography data reveal that the SWIR 46.0°E to 52.0°E segment is a V-shaped shallow domain (with an amplitude of nearly 2 km) similar to other ridges related to hotspots (Sauter et al., 2009). In the north-south direction of 47.0°E to 49.5°E segment, this V shape has a constant width of about 100 km. The width of the shallow domain gradually narrows from 49.5°E to the east. Based on the crustal age identified from the magnetic data, Sauter et al. (2009) suggested that this shallow domain began between 11.0 and 8.0 Ma and gradually propagated from west to east between 8.1 and 4.2 Ma with a speed of up to 30 mm/a, more than twice the spreading rate of the SWIR. In addition, the fault scarp of the shallow domain is very steep facing the off-axis direction, indicating an extremely sudden magmatism. With the spreading of the SWIR, the relict shallow domain at the western end of the V shape is symmetrically distributed. At the eastern end of the V shape, Segment 27 is one of several segments absent rift valleys (following the nomenclature of Cannat et al., 1999) with several flat-topped volcanoes. Its geophysical characteristics are similar to the slow-spreading MAR and may be the center of the present magmatism (Mendel et al., 2003). In the off-axis region, the paleo-ridge discontinuities suggest different segmentations before the magmatism and the present (Cannat et al., 1999), indicating that this intensive magma supply may lead to the segmentation change of the SWIR.

2 Data and results

2.1 Data sources

Bathymetry, gravity, sediment thickness, and crustal age are used to calculate the RMBA and the residual isostatic topography anomalies. The tomography model is from Debayle and Sambridge (2004). Bathymetry data are the latest 1′×1′ satellite altimetry-derived data (Topo-V11.1) from Smith and Sandwell (1997). Figure 1 shows that along the SWIR, available multi-beam data from cruises are added (Cannat et al., 1999; Sauter et al., 2004). In regions with complex topography, the data, being significantly more accurate than previous versions, are suitable for studying the mid-ocean ridges and seamounts with complex topographic variations. Compared with multi-beam data, the confidence of Topo-V11.1 can reach 96% (Zhang et al., 2011).

Figure 2 shows that the 18.1-version gravity data (FAA-V18.1), based on Sandwell and Smith (1997). Compared with previous versions, three corrections are used to reduce errors in FAA-V18.1: the raw waveforms from the ERS-1 and Geosat/GM missions are re-tracked, resulting in improvements in the range precision of 40% and 27%, respectively; the EGM2008 global gravity model is used as a reference field to provide a seamless gravity transition from

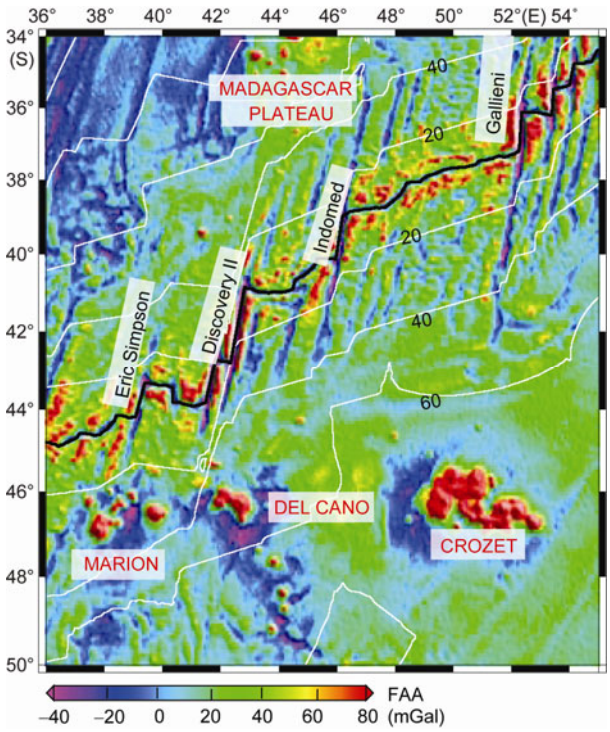

Figure 2 The free air anomalies of the Southwest Indian Ocean. Crustal ages are in black numbers; hotspots and plateaus are labeled in red; and major transform faults are labeled in black.

land to ocean; and a biharmonic spline interpolation method is adopted to construct residual vertical deflection grids (Sandwell et al., 1997). Comparisons between shipboard gravity and the global gravity grid show errors ranging from 2.0 mGal in even seafloor areas (the Gulf of Mexico) to 4.0 mGal in areas with rugged seafloor topographies.

The data of the crustal ages are the 2′×2′ oceanic crustal age data released by Müller et al. (2008). The error is less than 2 Ma in 58.9% of the study area and less than 5 Ma in 93.7% of the area.

The sediment thickness is the 5′×5′ gridded data provided by Divins[1)]. These data were compiled from the published sediment thickness isopach map, DSDP, and ODP, as well as the NGDC, IOC, and GAPA projects.

Debayle and Sambridge (2004) added the prior information in the 1°×1°×20 km Rayleigh wave model to handle the deficient data in the southern hemisphere owing to the scarce observation station, and to improve the reliability of the inversion model. Azimuthal anisotropy is added in the inversion to improve the lateral resolution of the upper mantle. S-wave velocity is more sensitive to temperature, so this model is more suitable for studying the variations of the mantle thermal structure.

2.2 RMBA and crustal thickness

The Parker method is adopted to subtract the effect of the density interfaces by layers to reveal more deep crust and mantle information (Parker et al., 1973). The mantle Bouguer anomalies (MBA) are calculated by subtracting from FAA the theoretical gravity effects of the water-sediment, sediment-crust, and crust-mantle interfaces assuming a constant density and a 6-km thick model crust. MBA primarily reflects the density variations caused by variations of crustal thickness and mantle temperature.

The oceanic lithosphere gradually cools and thickens while spreading away from spreading center, leading to an increasing density. The layered plate model is adopted to calculate the temperature of the lithosphere to remove the effect of lithospheric cooling. The density variations are obtained by assuming the thermal expansion coefficient (3.5×10^{-5} /K). The density variations are distributed within the whole lithosphere rather than to a specific density interface, so the whole lithosphere (150 km) is divided into 10 layers. The density variation of each layer is converted to the density contrast of the Moho interface, as shown in eq. (1):

$$h_1=15\times\Delta\rho/(3.3-2.7), \tag{1}$$

where h_1 is the height of each layer and $\Delta\rho$ is the average density variation.

The gravity effects of these 10 layers are summed to obtain the total effect of lithospheric cooling. Figure 3 shows

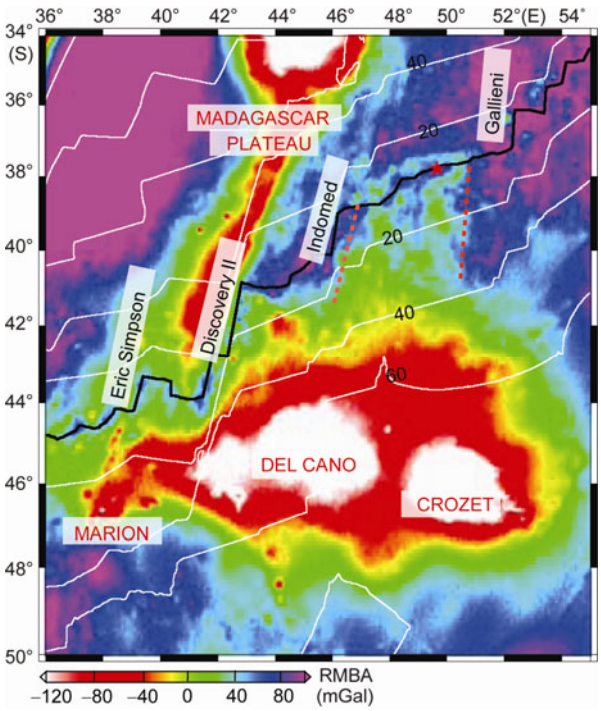

Figure 3 Residual mantle bouguer anomaly. The channel of the ridge-hotspot interaction is shown as the red dotted line, the crustal ages are labeled in black, and the hotspots, plateaus, and transform faults are labeled in red and black, respectively.

that the RMBA, which is obtained by subtracting this effect from the MBA, indicates the variations of the crustal thickness or the mantle temperature or both.

In the region of 46.0°E to 52.0°E, the negative RMBA shows a V-shaped anomaly zone from the west to the east, corresponding to the shape of the shallow domain. The V-shaped area corresponds to RMBA of approximately −40 mGal. Nevertheless, compared with topography, the RMBA's V shape is more prominent and slightly smaller. The V-shaped negative anomaly zone of the RMBA is between 47.2°E on the west and Segment 27 (about 50.5°E) on the east. Rift valleys exist on the eastern and western sides of Segment 27, indicating that the magma supply decreased or disappeared in these areas. Segment 27 is the center of the present magmatism.

When ascribing the variations of the RMBA to the crustal thickness, the maximum crustal thickness variation is obtained by inversion (part of the effect of the mantle temperature is converted to the variations of crustal thickness). The crustal thickness variations are calculated by downward continuation (Van Ark et al., 2004), as shown in eq. (2).

$$M(k)=\frac{\exp(Kz_{CR})}{2\pi G(\rho_m-\rho_c)}B(k)C(k), \tag{2}$$

1) http://www.ngdc.noaa.gov/mgg/sedthick/sedthick.html

where z_{CR} is the mean crustal root depth below sea level and $C(k)$ is a low-pass cosine filter. The downward depth is 10 km (4-km mean water depth and 6-km constant crustal thickness). The longest and shortest wavelength of the filter is 135 and 25 km, respectively. Figure 4 shows the crustal thickness.

2.3 Residual tomography model

The oceanic lithosphere is generally 100–150 km thick. Given the relatively thin oceanic lithosphere at the spreading center, the tomography data are taken at a depth of 75 km, as shown in Figure 5(a). There are three prominent features are included in the figure. The first is the slowest seismic velocity on the axis. With the aging of the crust, the seismic velocity symmetrically increases toward both sides of the axis, indicating the gradually cooling lithosphere. Second, the seismic velocities of intermediate spreading SEIR and CIR are significantly slower than that of the SWIR, indicating that the thermal structure of the lithosphere changes with the spreading rate. Third, the hotspot areas all correspond to the low-velocity areas, whereas the major transform faults correspond to the high-velocity areas. In addition, the transform faults have a significant role in the segmentation of the lithospheric thermal structure even at a depth of 75 km.

The part in which the seismic velocity varies with age is removed to highlight the effect of hotspots (Figure 5(b)). The curve related to age and velocity is obtained by fitting all the data in the study area, as shown in Figure 5(b). After the removal of this part from the model, the residual seismic velocity at the depth of 75 km is shown in Figure 5(c).

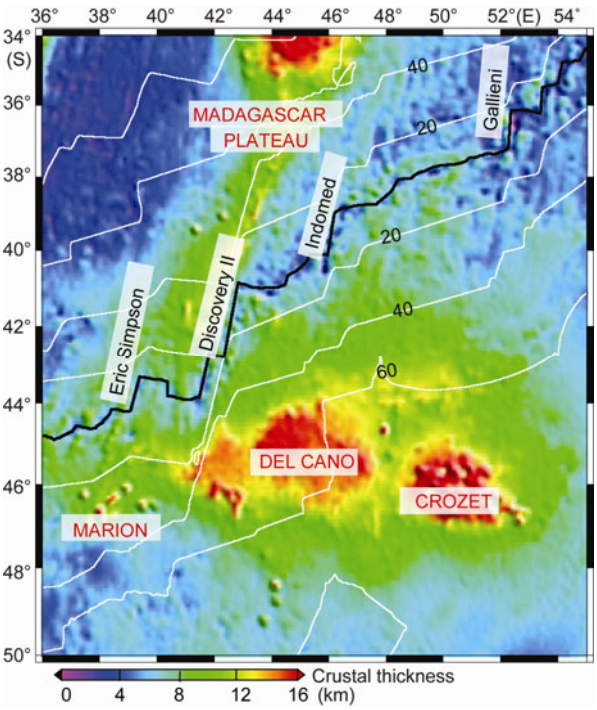

Figure 4 The gravity-derived crustal thickness. The crustal ages are labeled in black; and the hotspots, plateaus, and transform faults are labeled in red and black, respectively.

2.4 The residual isostatic topography anomaly

Similar to the calculation of RMBA, the residual bathymetry reflecting the magmatism at the time of crust formation can be obtained by removing the sediments and the lithospheric cooling effect from the observed water depth (Ito et al., 2003; Zhang et al., 2011). With the residual bathymetry and the crustal thickness, the corresponding isostatic topography can be calculated based on the Airy isostatic model. By removing the isostatic topography from the residual bathymetry, the residual isostatic topography anomaly can be obtained. The residual isostatic topography anomaly reveals the extent of deviation from the Airy isostatic equilibrium, as shown in Figure 6. Due to the thin lithosphere close to the axis, the residual isostatic topography has significantly low amplitude at those areas, tending to exhibit a locally isostatic equilibrium. In the whole map, the most prominent uncompensated region is the insider corner of the transform faults. The pronounced high-residual isostatic topography anomalies show the under-compensation in these areas and are consistent with the characteristics of the thinner crustal thickness. In addition, many seamounts have the characteristics of the conjunction positive and negative anomalies, similar to the regional equilibrium state (Vidal et al., 2004). The Marion-Del Cano-Crozet Area is a huge uplift in topography, but the Del Cano Rise has very low amplitude residual isostatic topography anomaly, which is consistent with the suggestion that the Del Cano Rise was created when the Marion hotspot was close to the SWIR (Zhang et al., 2011). There are higher residual isostatic topography anomalies than the surrounding areas on the Marion and Crozet hotspots, suggesting that the lithosphere has certain mechanical strength when those seamounts formed, leading to the regional isostatic compensation.

2.5 The magnetic data and the magnetic source layer model

To investigate the tectonic features of Area A, four gravity and magnetic profiles are chosen for geological modeling (see Figure 7 for the location). The magnetic data is sampled with G880 Cesium Magnetometer in the DY-20 cruise (DY115-20) with the satellite difference GPS for positioning. To reduce the effect of ship magnetism, the sensor is towed 300 m away from the ship (over three times the ship's length) during measurement. After the position correction, IGRF (2005) is used to correct the regional magnetic field. The final magnetic anomaly data is sampled at 6-s intervals, about 18 m per point (the ship speed is assumed to be constantly at 6 knots).

The Modmag software is used to build models (Mendel

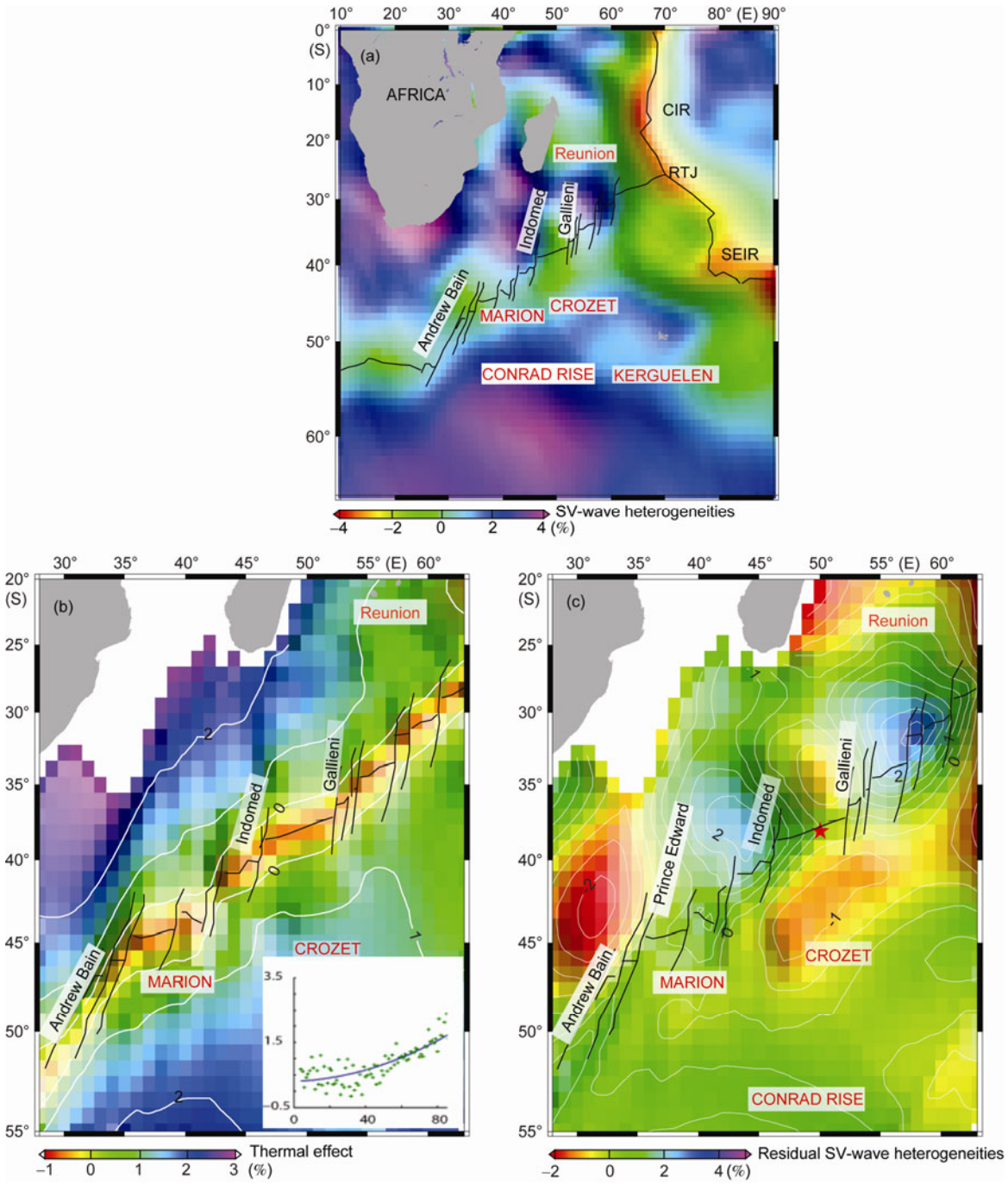

Figure 5 SV-wave heterogeneities under the SWIR at 75 km. (a) The original data from Debayle and Sambridge (2004); mid-ocean ridges, major transform faults, and fracture zones are represented by the black curve. CIR is the central Indian ridge, SEIR is the Southeast Indian ridge, and RTJ is the Rodrigues triple junction. (b) The seismic velocity model caused by the cooling of the lithosphere. See the illustration for the curve relating to age and seismic velocity. (c) The residual seismic velocity anomaly after correction. The red asterisk marks the location of Area A hydrothermal vent.

et al., 2005). Modmag considers different spreading rates, asymmetric spreading, and ridge jumps; however, it only considers constant magnetic source thickness. To establish a more realistic model, the software was modified in this study to deal with variable magnetic source thickness. The specific modeling process is as follows:

(1) The seafloor and the Moho are drawn based on the bathymetry data and gravity derived crustal thickness. The thickness of the initial magnetic source layer (basalt, 2A) is calculated based on the variation of the crustal thickness. The rest parts were dikes and gabbros (all assumed to be non-magnetic). According to Sauter et al. (2004), all magnetic source layers are assumed to be constant 0.5 km for the Brunhes period.

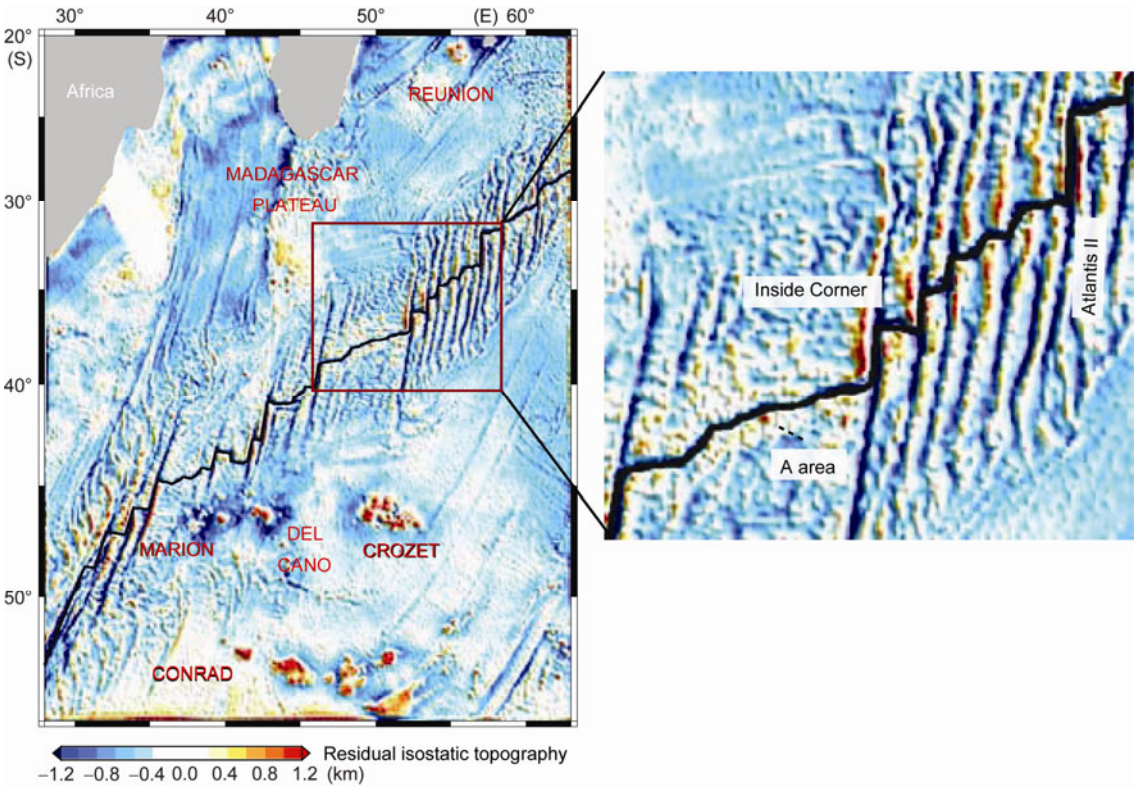

Figure 6 The residual isostatic topography anomaly.

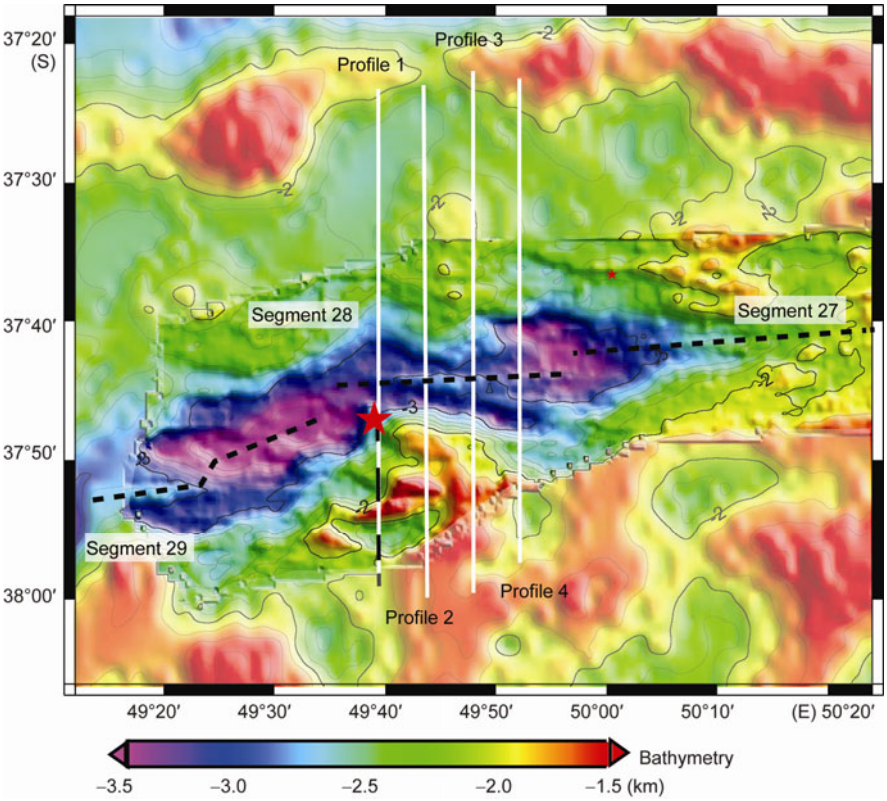

Figure 7 Bathymetry of Local Area A. The satellite altimetry-derived bathymetry data are covered with a transparent box. The rest are multi-beam data. The white line indicates the profile location of the magnetic data, the black dotted line indicates the axis, and the number indicates the second-order segments.

(2) The spreading rate and asymmetry of the SWIR are calculated based on the crustal ages determined by the magnetic anomaly. The polarity and magnetization are set to each magnetic source layer based on the geomagnetic reversal timescale (Cande et al., 1995). According to the magnetization of MAR's magnetic source layer, the magnetization of the young magnetic source layer within the Brunhes/Matuyama period (0.78 Ma) is assumed to be 20 A/m, and the rest to be ± 4 A/m.

(3) The magnetic effect of each magnetic source layer is calculated, integrated, and compared with the observation. The thickness of the magnetic source layer was adjusted carefully to make the calculated data fit the observed data. The observed and calculated data of each profile are shown in Figure 8.

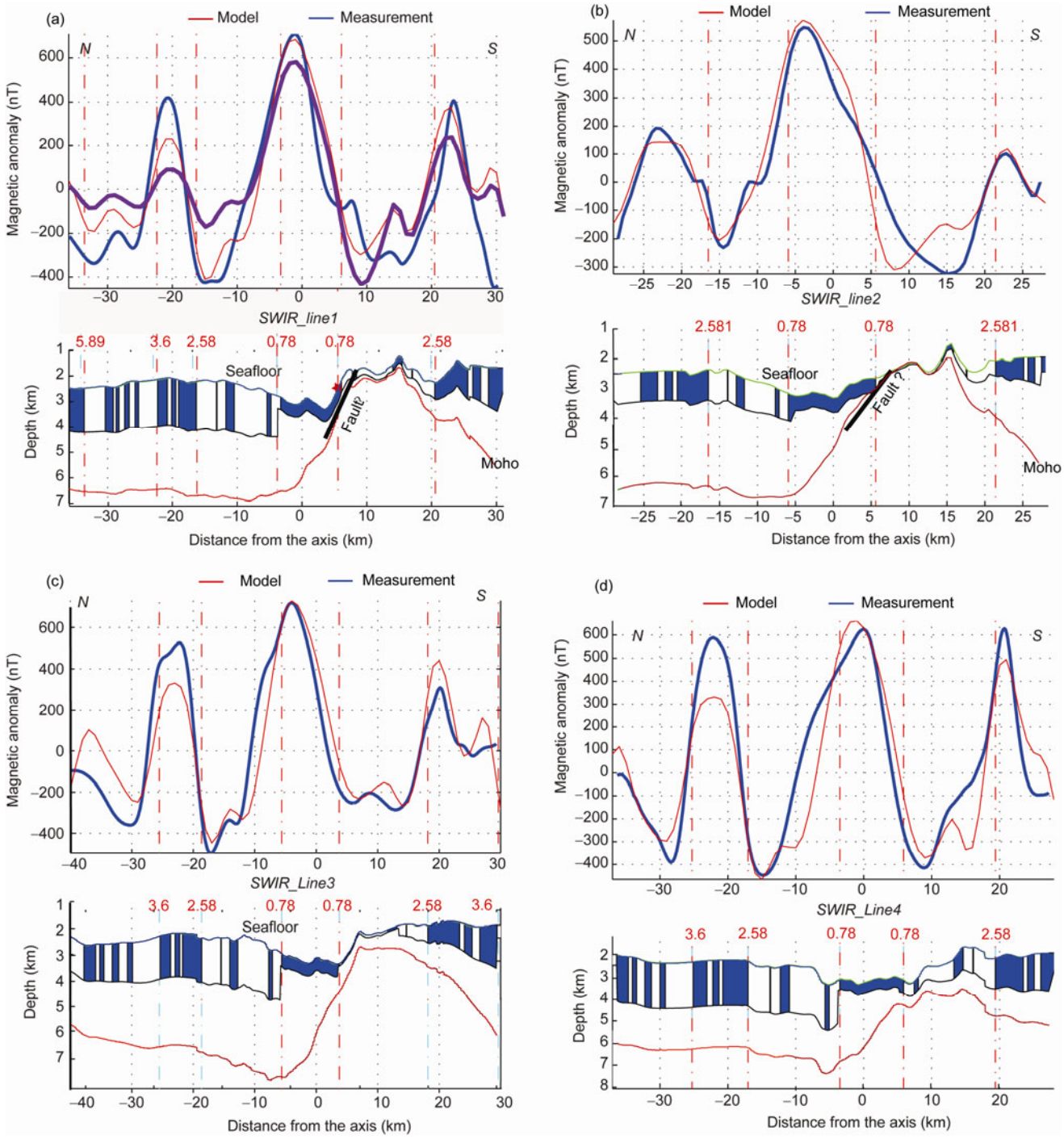

Figure 8 The geological model based on gravity and magnetic profiles. (a) Profile 1. Observation and best-fit data are indicated with blue and red curves, respectively. The fitted data with constant source layer thickness (0.5) are indicated by the purple curve. The detachment fault is marked on the profile. (b) Profile 2. The line crosses the Area A vent. (c) Profile 3. (d) Profile 4.

3 Discussion

3.1 Formation of the V-shaped anomaly

The symmetrical crust structure is formed on most of spreading center while spreading away. The RMBA differences on the paleo-ridges (along the isochrones) can be explained as the results of the subsequent alteration. The difference between the present spreading center and the paleo-ridge reflects the temporal variation of melting anomaly intensity. If we ascribe all melting anomaly differences to hotspot effect, the former difference reflects the underplating of the hotspot, whereas the latter shows the temporal variation of the hotspot effect along the spreading center.

The profiles along the paleo-ridge in three stages, namely, before the supply, supply beginning, and most intensive supply, are adopted to analyze the formation of intensive magma supply along the SWIR 46.0° to 52.0°E. Sauter et al. (2009) suggested that the effect of magma supply on SWIR began between 11 and 8 Ma. However, it has been obviously weakened at present. As shown in Figure 1(b), the most intensive magmatism is between the magnetic anomaly C3n.y (4.180 Ma) and C3An.y (5.894 Ma), at about 5 Ma. Therefore, three isochrones, namely, 20, 10, and 5 Ma, are selected in this study, as shown in Figure 9.

The crusts along the symmetrical isochrones are generated from the same axis. Normally, they have similar RMBA anomalies and crustal thickness. However, at 20 Ma, the most prominent feature is the RMBA on the south axis, which is lower than that of the north side along the entire isochrones. The largest difference is in the 47.5° to 51.5° E region, with a mean difference of more than 40 mGal. Given the melting anomalies amplitude and the locations of Marion and Crozet (on the south of SWIR), the low RMBA anomaly (or the thickening crust) may be caused by the underplating effect of the hotspots. In the 47.5° to 51.5°E area, the RMBA along the present spreading center is between the RMBAs on the north and south sides. The high RMBA on the north side indicates that the magmatism was relatively weak at that time and the hotspots had little effect on SWIR. By contrast, the present RMBA along the SWIR indicates intensive magmatism. At 10 Ma, the RMBA on the north side of the 47.5° to 50.0°E area significantly decreased, indicating that magmatism began to intensify, resulting in the decreased RMBA difference between the north and the south. West of 46° to 47.5°E, the RMBAs on both the south and north sides increased, indicating that magmatism was limited between 47.5°E and 50.0°E. Thus, it did not affect the east and west sides. In the 47.5° to 50.0°E region, the present RMBA along the spreading center is higher than that on both the north and the south sides, indicating that the magmatism weakened. The RMBA along the present spreading center shows the lowest value at 50.5°E, indicating that the present magmatism center propagated to Segment 27. At 5 Ma, the RMBA on the south side of 46.0° to 47.5°E significantly increased, suggesting that magmatism weakened. This phenomenon may be related to the inside corner of the Indomed transform fault. East of 47.5°E, the RMBA on the south side increased slightly, which may be ascribed to the weakening of the underplating while the hotspot gradually moved away from the SWIR. The RMBA on the north side decreased, indicating that magmatism along the paleo-ridge was further enhanced. Especially between the 49.0° to 51.0°E region, the reduced amplitude of the RMBA is up to 40 mGal. The lowest RMBA at 50.5°E is close to its present RMBA, indicating that 10–5 Ma is the period during which the magmatism rapidly propagated from the west to the east along the SWIR.

The RMBA on the south side of SWIR is related to the hotspot-ridge distance, so it has been gradually increasing from 20 Ma to the present. The underplating effect has gradually weakened. As shown on the north-side profile of SWIR, the robust magma supply begins at 10 Ma and reaches the highest intensity at 5 Ma. The intensive magmatism only acts between 47.5°E and 50.0°E and propagates from the east to the present location. Intensive magmatism seems to have no effect on the west region from 46° to 47.5°E.

3.2 The ridge-hotspot interaction channel

On a larger scale, the V-shaped area connects with the Marion-Del Cano-Crozet uplift by a low-RMBA zone (50 mGal lower than the surrounding area on the average) whose width is smaller than its length (approximately 300 km), as shown in Figure 3. The west side of this low-value zone is blocked by the Indomed transform fault and is consistent with the transform fault barrier on the ridge-hotspot interaction proposed by Georgen et al (2001). The asymmetry of RMBA along the paleo-ridge on both the north and the south sides gradually weakens with increase in the hotspot-ridge distance. Along the SWIR, this V shape propagates to the present magmatism center from west to east. These phenomena are consistent with the characteristics of the ridge-hotspot interaction, so this low-RMBA zone may be the channel of the ridge-hotspot interaction. From the Marion-Del Cano-Crozet uplift region to the SWIR, this channel is restricted by the Indomed transform fault on the west and connected to 50.0°E on the east with constant width of about 240 km.

Marion-Del Cano-Crozet forms a huge uplift with a diameter of about 2000 km in the southwest Indian Ocean. Georgen et al. (2009) showed that under the barrier effect of large transform faults, the effect of Marion significantly reduced upon crossing the Discovery II transform fault. The Del Cano Rise is a plateau formed during the SWIR-Marion hotspot interaction (Zhang et al., 2011). However, it no longer exhibits any activity. The Crozet hotspot is most likely the source of the robust magmatism along the 46° to 52°E region, consistent with the results by Sauter et al.

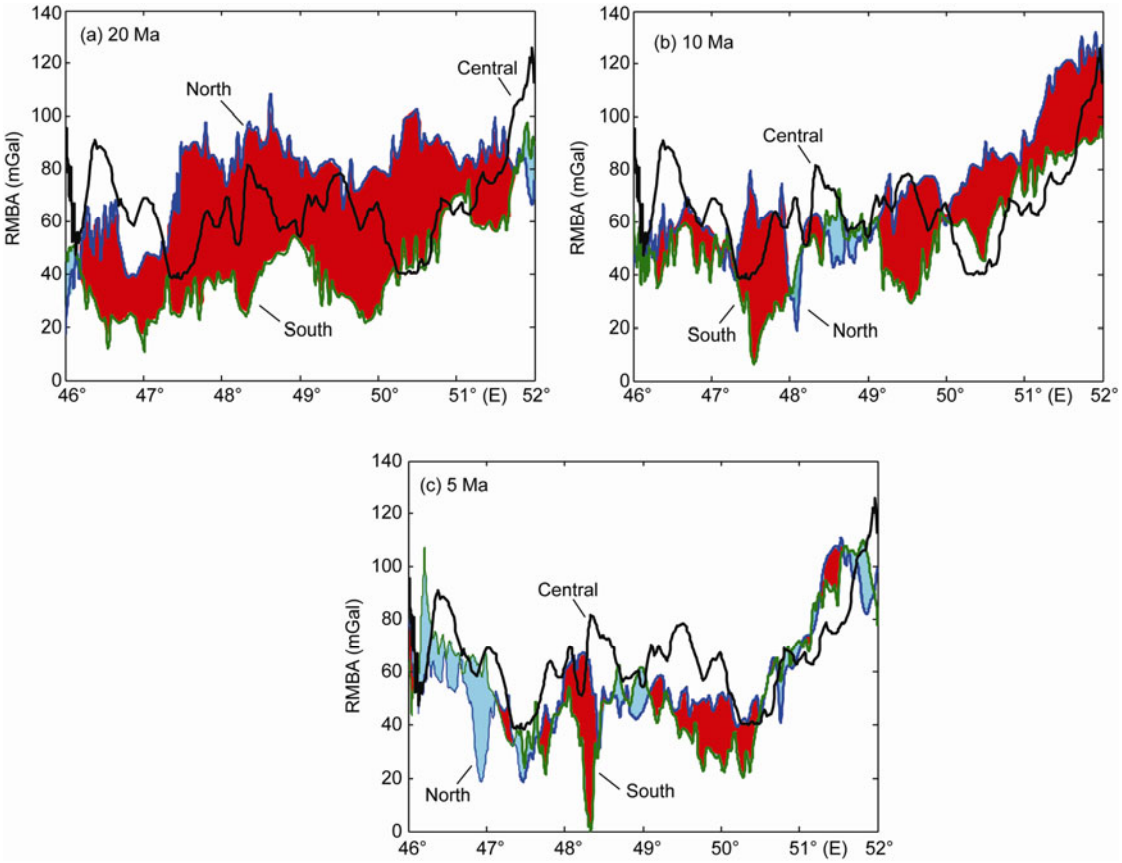

Figure 9 The RMBA along the isochrones. (a) The RMBA along the 20 Ma isochrones. The blue curve represents the RMBA on the north of the axis; the green curve represents the RMBA on the south of the axis; the black curve represents the RMBA along the present spreading center; the red area indicates that the RMBA on the south side is lower than that on the north side; and the blue area indicates that the RMBA on the south side is larger than that on the north side. (b) The RMBA along the 10 Ma isochrones. (c) The RMBA along the 5 Ma isochrones.

(2009) according to topography data.

A previous study on the Iceland and Reykjanes ridges show that the effects of the hotspots affect the rheology of the ridges, resulting in the permeability reduction of the lithosphere; thus, the probability of creating a hydrothermal vent in the hotspot-affected area is low (Chen et al., 1999). The existing rift valley along the Area A vent segment indicates that the current magmatism is significantly weakened. The effect of Crozet on SWIR is not as robust as that of Iceland on the Reykjanes ridge. In this case, Crozet's effect along SWIR provides the sufficient heat source for the hydrothermal vent, but not intensive enough to diminish the crustal permeability and block water circulation completely.

3.3 The ridge-hotspot interaction channel from tomography

The depth of the ridge-hotspot interaction channel has an equal significance with its horizontal position. The depth of origin of the hotspot (mantle plume) has many possibilities (core-mantle boundary, 660 km or the base of the lithosphere). The hotspot-ridge interaction also has many possible geometric forms, such as pipe-like channels or broad expanding gravity currents. Owing to the poor vertical resolution of the gravity, we adopt the tomography data to investigate the state of the base of lithosphere in the SWIR region.

As shown in Figure 5, there are two SV-wave anisotropy anomalous zones whose amplitudes are more than 1% at 75 km (relative to the velocity at 75 km in the PREM model, 4.39 km/s; Dziewonski et al., 1981). One is near the Prince Edward transform fault at 36.5°E and the other is at the center of Segment 27 (50.5°E). These two negative anomalies indicate the high-temperature mantle. South of SWIR, the anomaly elongates to the Crozet from Segment 27. Its horizontal position is close to the SWIR-Crozet interaction channel (Figure 3) from the gravity data. Across the SWIR, this low velocity anomaly changes from the northeast direction on the south side of SWIR to the northwest direction and is almost consistent with the spreading direction. SWIR may alter the channel of hotspot effect.

From the cross-section taken by Sauter et al. (2009), there are significant low-seismic velocity anomalies between the Crozet and Segment 27 in SWIR. The thermal anomaly activities at 150-km depth coincide with the horizontal ridge-hotspot interaction channel, indicating that the

ridge-hotspot interacts throughout the lithosphere. The cross-section also shows that no low velocity anomaly resembles the mantle plume under Crozet. The model of Debayle and Sambridge probably cannot distinguish mantle plumes with approximately 200-km diameter (Sauter et al., 2009). However, Crozet itself may be the shallow hotspot from the base of the lithosphere.

3.4 The tectonic characteristics of the Area A hydrothermal vent

As shown in Figure 6, in the 46° to 52°E region, all areas are in complete isostatic equilibrium except Area A. Area A is on the scarp of the rift valley at the intersection of the discontinuity between Segments 28 and 29. In areas with the crustal age between 0 and 2.6 Ma, the topography and crustal thickness on both sides of the SWIR show a significant asymmetry. Compared with the north side of the SWIR, the south side of Area A is 0.5 km shallow, whereas the corresponding crustal thickness is 2.9 km thinning, resulting in 1.6 km residual isostatic anomaly topography on the south side, as shown in Figure 10. Along SWIR, such significant deviation of isostatic compensation is only discovered at the inside corner of transform faults. The shallowest residual isostatic topography at the inside corner of the Atlantis II transform fault is 2.9 km with an average of 1.5 km. The inside corner of the transform fault usually corresponds to the footwall of the detachment fault, so such significant deviation of isostatic compensation may be related to detachment fault.

The thinning magnetic source layer in Area A also implies that its tectonic feature is similar to that of detachment faults. The four forward magnetic profiles show that the

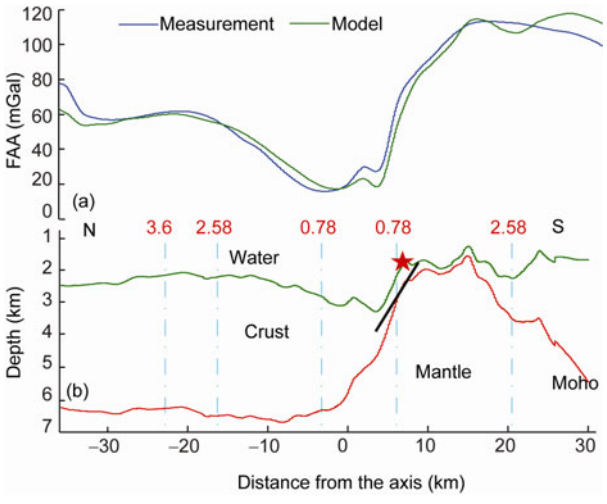

Figure 10 The forward gravity effect and crustal model across the vent. (a) Gravity forward profile: the root mean square value of the observation and calculation is 6.0 mGal; (b) crustal thickness: the crustal ages are marked with numbers and the vent position is indicated with asterisk.

magnetic source layers at the south of Area A (0.78–2.58 Ma) are significantly thinning, as shown in Figure 8. There are several explanations for this phenomenon, such as the combined effect of frequently reversed magnetic anomalies, abrupt changes of the Earth's magnetic field, reduction of magma supply, thermal alteration, hydrothermal alteration, and tectonic thinning. The first three take place during the formation of the crust, whereas the latter three occur after the formation. The calculation based on constant magnetic source thickness (0.5 km) and reversal timescale are inconsistent with the observation (Figure 8(a)). Within 2.58 Ma, the Earth's magnetic field has no significant change, so this low magnetization is not caused by the magnetic reversal or the changes of the Earth's magnetic field. The thermal alteration after the formation of the crust is also excluded in this study because off-axis magmatism is rare. The hydrothermal alteration can instantly lead to low magnetization. The analysis of near-bottom magnetometer data by Zhu et al. (2010) shows that the hydrothermal alteration in Area A is only about hundreds of meters, which is inconsistent with the range of 10 km. Given the thick crust on the north side of SWIR, the magmatism effect is also excluded. Thus, we ascribe the thinning of the magnetic source layer to tectonic extension.

The four profiles have the same trends. The magnetic source layer on the south side is much thinner than that on the north side. The magnetic source layers of Profiles 1–3 are thinner than normal thickness (0.5 km) on the south of SWIR. The thinning magnetic source layer (less than 0.2 km) from the profiles is approximately 7 km along the axis and approximately 15 km in the spreading direction. The profile (Profile 2) across the vent has the thinnest thickness on its south part, as shown in Figure 8(b). Along this profile, the thinning magnetic source layer corresponds to the shallow high-velocity zone revealed by OBS (Zhao et al., 2011). Given the crustal thickness, the isostatic compensation, and the characteristics of the magnetic source layer, Area A may be under the control of a detachment fault.

In topography, Area A is greatly different from the Megamullions observed in other detachment faults (Smith et al., 2006). According to the OBS data, the shallow high-velocity area is not continuous under SWIR, so the thinning magnetic source layer may be caused by some detachment faults of incomplete evolution. The detachment fault under Area A may be at its initial evolution stage.

A long-lived and episodically active detachment (Tucholke et al., 2008) may provide sufficient permeability for continuous water circulation of the hydrothermal vent. If the detachment fault evolved under the Area A vent, its tectonic characteristics will be similar to those of TAG. Thus, it will have good prospects for massive sulfide deposits. The hydrothermal alteration area measured by a near-bottom magnetometer by Zhu et al. (2010) showed that the low crustal magnetization zone in Area A is up to 9×10^4 m^2, which is larger than that of TAG. The detachment fault may be an

important control factor. This finding implies that the tectonic role is an important control factor for hydrothermal vents on ultra-slow spreading ridges.

4 Conclusions

The significant robust melting anomaly, the V-shaped RMBA, the topographical features along the SWIR, and the RMBA differences along the isochrones suggest that the study area is affected by a hotspot. The RMBA and the residual seismic velocity anomalies indicate the horizontal and vertical range of the SWIR-Crozet interaction channel. The intensive magmatism related to the SWIR-Crozet interaction provides abundant heat source for Area A hydrothermal vent.

At the Area A hydrothermal vent, the shallow seafloor and the thinning crust lead to the deviation of isostatic equilibrium. The residual isostatic topography anomalies are similar to those of the transform fault insider corner. The magnetic data show that the thinning magnetic source layer at the south of Area A is about 7 km × 15 km, which is ascribed to the tectonic extension of the detachment fault. The intensive tectonic processes in Area A can provide increased crustal permeability to the hydrothermal circulation, resulting in more possibilities for forming large hydrothermal sulfide deposits.

We are grateful to Dr. Li Jiabiao in the Second Institute of Oceanography (SIO), SOA for providing favorable conditions and constructive suggestions for this study. We benefit greatly from discussions with Dr. Sun Zhen and Dr. Zhao Minghui in the South China Sea Institute of Oceanology, Chinese Academy of Sciences and Dr. Han Xiqiu and Dr. Ruan Aiguo in SIO, SOA. Tan Yonghua in SIO, SOA collected the magnetic data. Most of the figures in this study were created with GMT software (Wessel & Smith, 1995). This work was supported by the National Natural Science Foundation of China (Grant No. 41106049) and Special Funding for the Basic Scientific Research (Grant No. JT1106).

Baker E T, Edmonds H N, Michael P J, et al. 2004. Hydrothermal venting in magma deserts: The ultraslow-spreading Gakkel and Southwest Indian Ridges. Geochem Geophys Geosyst, 5: Q08002, doi: 10.1029/2004GC000712

Cande S C, Kent D V. 1995. Revised calibration of the geomagnetic polarity timescale for the late cretaceous and cenozoic. J Geophys Res, 100: 6093–6095

Cannat M, Rommevaux-Jestin C, Sauter D, et al. 1999. Formation of the axial relief at the very slow spreading Southwest Indian Ridge (49° to 69°E). J Geophys Res, 104: 21825–21843

Cannat M, Sauter D, Mendel V, et al. 2006. Modes of seafloor generation at a melt-poor ultraslow-spreading ridge. Geology, 34: 605–608

Charvis P, Recq M, Operto S, et al. 1995. Deep structure of the northern Kerguelen Plateau and hotspot related activity. Geophys J Int, 122: 899–924, doi: 10.1111/j.1365-246X.1995.tb06845.x

Chen Y J, Lin J. 1999. Mechanisms for the formation of ridge-axis topography at slow-spreading ridges: A lithospheric-plate flexural model. Geophys J Int, 136: 8–18, doi: 10.1046/j.1365-246X.1999.00716.x

Curray J R, Munasinghe T. 1991. Origin of the Rajmahal Traps and the 85°E Ridge: Preliminary reconstructions of the trace of the Crozet hotspot. Geology, 19: 1237–1240

Debayle E, Sambridge M. 2004. Inversion of massive surface wave data sets: model construction and resolution assessment. J Geophys Res, 109: B02316, doi: 10.1029/2003JB002652

Dick H J B, Lin J, Schouten H. 2003. An ultraslow-spreading class of ocean ridge. Nature, 426: 405–412

Dziewonski A, Anderson D. 1981. Preliminary reference Earth model. Phys Earth Planet Int, 25: 297–356

Georgen J E, Lin J, Dick H J B. 2001. Evidence from gravity anomalies for interactions of the Marion and Bouvet hotspots with the Southwest Indian Ridge: Effects of transform offsets. Earth Planet Sci Lett, 187: 283–300

Goslin J, Patriat P. 1984. Absolute and relative plate motions and hypotheses on the origin of five aseismic ridges in the Indian Ocean. Tectonophys, 101: 221–244

Ito G, Lin J, Graham D. 2003. Observational and theoretical studies of the dynamics of mantle plume-mid-ocean ridge interaction. Rev Geophys, 41: 1017, doi: 10.1029/2002RG000117

Lin J, Zhang C. 2006. The first collaborative China-international cruises to investigate mid-ocean ridge hydrothermal vents. Inter Ridge News, 15: 33–34

Mendel V, Sauter D, Rommevaux-Jestin C, et al. 2003. Magmatic-tectonic cyclicity at the ultra-slow spreading Southwest Indian Ridge: Evidence from variations of axial volcanic ridge morphology and abyssal hills pattern. Geochem Geophys Geosyst, 4: 9102, doi: 10.1029/2002GC000417

Mendel V, Munschy M, Sauter D, et al. 2005. MODMAG, a MATLAB program to model marine magnetic anomalies. Comput Geosci, 31: 589–597

Montelli R, Nolet G, Dahlen F, et al. 2004. Finite-frequency tomography reveals a variety of plumes in the mantle. Science, 303: 338–343

Müller R D, Sdrolias M, Gaina C, et al. 2008. Age, spreading rates, and spreading asymmetry of the world's ocean crust. Geochem Geophys Geosyst, 9: Q04006, doi: 10.1029/2007GC001743

Parker R L. 1973. The rapid calculation of potential anomalies. Geophys J Roy Astron Soc, 31: 447–455, doi: 10.1111/j.1365246X.1973.tb06513.x

Recq M, Goslin J, Charvis P, et al. 1998. Small-scale crustal variability within an intraplate structure: The Crozet Bank (southern Indian Ocean). Geophys J Int, 134: 145–156

Sandwell D T, Smith W. 1997. Marine gravity anomaly from Geosat and ERS 1 satellite altimetry. J Geophys Res, 102: 10039–10054, doi: 10.1029/96JB03223

Sauter D, Carton H, Mendel V, et al. 2004. Ridge segmentation and the magnetic structure of the Southwest Indian Ridge (at 50°30′E, 55°30′E and 66°20′E): Implications for magmatic processes at ultraslow-spreading centers. Geochem Geophys Geosyst, 5: Q05K08, doi: 10.1029/2003GC000581

Sauter D, Cannat M, Meyzen C, et al. 2009. Propagation of a melting anomaly along the ultraslow Southwest Indian Ridge between 46° E and 52°20′E: Interaction with the Crozet hotspot? Geophys J Int, 179: 687–699

Smith D K, Cann J, Escartin J. 2006. Widespread active detachment faulting and core complex formation near 13° N on the Mid-Atlantic Ridge. Nature, 442: 440–443, doi: 10.1038/nature04950

Smith W H F, Sandwell D T. 1997, Global sea floor topography from satellite altimetry and ship depth soundings. Science, 277: 1956–1962

Tao C, Lin J, Guo S, et al. 2012. First active hydrothermal vents on an ultraslow-spreading center: Southwest Indian Ridge. Geology, 40: 47–50

Tucholke B, Behn M, Buck W R, et al. 2008. Role of melt supply in oceanic detachment faulting and formation of megamullions. Geology, 36: 455–458, doi: 10.1130/ G24639A

Van Ark E, J Lin. 2004. Time variation in igneous volume flux of the Hawaii-Emperor hot spot seamount chain. J Geophys Res, 109:

B11401, doi: 10.1029/2003JB002949
Vidal V, Bonneville A. 2004. Variations of the Hawaiian hot spot activity revealed by variations in the magma production rate. J Geophys Res, 109: B03104, doi: 10.1029/2003JB002559
Wang T, Lin J, Tucholke B et al. 2011. Crustal thickness anomalies in the North Atlantic Ocean basin from gravity analysis. Geochem Geophys Geosyst, 12: Q0AE02, doi: 10.1029/2010GC003402
Wessel P, Smith W H F. 1995. New version of the Generic Mapping Tools released. EOS Trans AGU, 76: 329
Zhang T, Lin J, Gao J. 2011. Interactions between hotspots and the Southwest Indian Ridge during the last 90 Ma: Implications on the formation of oceanic plateaus and intra-plate seamounts. Sci China Ser D-Earth Sci, 54: 1177–1188, doi: 10.1007/s11430-011-4219-9
Zhao M, Zhang J, Qiu X, et al. 2011. Preliminary results of 3D seismic structure in the Southwest Indian Ocean Ridge (37°50'S). AGU Fall Meeting, Abstract #S41A-2146
Zhu J, Lin J, Chen Y J, et al. 2010. A reduced crustal magnetization zone near the first observed active hydrothermal vent field on the Southwest Indian Ridge. Geophys Res Lett, 37: L18303, doi: 10.1029/2010GL043542